Biochar-zeolite modified super sulphate cement as a high-performance, sustainable and high-efficiency CO_2 sequestration cementitious material

Miao, Jianxiong; Xiao, Shuai; Zhou, Yang; Chen, Wentao; Jin, Yanji; Cheng, Luqing; Chang, Cheng; Zhang, Hao

DOI
10.1016/j.conbuildmat.2025.142475

Publication date
2025

Document Version
Final published version

Published in
Construction and Building Materials

Citation (APA)
Miao, J., Xiao, S., Zhou, Y., Chen, W., Jin, Y., Cheng, L., Chang, C., & Zhang, H. (2025). Biochar-zeolite modified super sulphate cement as a high-performance, sustainable and high-efficiency CO_2 sequestration cementitious material. *Construction and Building Materials*, *490*, Article 142475. https://doi.org/10.1016/j.conbuildmat.2025.142475

Construction and Building Materials 490 (2025) 142475

Contents lists available at ScienceDirect

Construction and Building Materials

journal homepage: www.elsevier.com/locate/conbuildmat

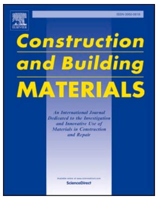

Biochar-zeolite modified super sulphate cement as a high-performance, sustainable and high-efficiency CO_2 sequestration cementitious material

Jianxiong Miao [a], Shuai Xiao [b,c,*], Yang Zhou [b,c], Wentao Chen [b,c], Yanji Jin [b,c], Luqing Cheng [b,c], Cheng Chang [d,**], Hao Zhang [c]

[a] *Department of Civil and Engineering, National University of Singapore, 117576, Singapore*
[b] *School of Materials Science and Engineering, Southeast University, Nanjing, Jiangsu 211189, China*
[c] *State Key Laboratory of Engineering Materials for Major Infrastructure, Southeast University, Nanjing 211103, China*
[d] *Department of Engineering Structures, Faculty of Civil Engineering and Geosciences, Delft University of Technology, Stevinweg 1, Delft 2628 CN, the Netherlands*

ARTICLE INFO

Keywords:
Carbon emissions reduction
Super sulfated cement
Hierarchical pore structure
CO_2 sequestration
Sustainable construction materials
Environmental sustainability

ABSTRACT

Cement production contributes 8 % of global industrial carbon emissions, underscoring the urgent need for innovative strategies to mitigate its environmental impact. Super Sulfated Cement (SSC) is a promising low-carbon alternative, but its carbon sequestration potential remains underexplored. This study integrates biochar and zeolite into SSC to create a near-zero-carbon, high-performance composite with hierarchical transport pathways, enhancing compressive and flexural strength by 63.1 % and 43.8 %. A comprehensive mechanism for the composite's carbon sequestration is proposed, leveraging biochar's tunnel-like channels and zeolite's nanopores, along with molecular sieve properties, to create a hierarchical pore structure. This structure facilitates CO_2 transmission to greater depths and enables lateral diffusion, increasing carbonation by 37 % and CO_2 uptake to 41.7 kg·CO_2/kg. Its Global Warming Potential is 51.08 kg·CO_2/kg, reducing emissions by 87 % and 51.1 % compared to Ordinary Portland Cement (OPC) and SSC, respectively. This study provides an innovative, scalable pathway to developing ultra-low-carbon cementitious materials, leveraging industrial and agricultural waste to enhance environmental sustainability. The findings offer actionable insights for advancing carbon capture technologies and achieving negative-carbon cement production.

Synopsis: Integrating biochar and zeolite into supersulfated cement enhances CO_2 sequestration, reducing life-cycle carbon emissions and addressing solid waste valorization and air quality challenges.

1. Introduction

It is estimated that carbon emissions from cement production account for nearly 8 % of global industrial emissions [1–3]. Carbon Capture and Storage (CCS) technology, which has gained widespread attention in recent years, can reduce system carbon emissions by solidifying CO_2 in cement through carbonation curing [4]. Due to the inherently high carbon emissions of Ordinary Portland Cement (OPC) [5], CCS can only reduce its carbon emissions by 15 %, and the net emissions of CO_2 still cannot be effectively reduced [6,7]. Thus, developing a low-carbon base system that also has high carbon sequestration capacity is of great significance.

Super Sulfated Cement (SSC), primarily composed of slag and gypsum, uses a small amount of cement as an activator to initiate the depolymerization of Ground Granulated Blast Furnace Slag (GGBS), forming a cementitious system whose strength is derived from calcium aluminate (AFt) and Calcium Silicate Hydrate (C-S-H) [8]. With a low carbon emission of 153.10 kg·CO_2/kg and a high carbonation potential, SSC exhibits significant carbon sequestration potential with negative emissions. [9,10]. When SSC is carbonated under 3-day curing conditions at 28 days, the carbonation depth can reach 8.1 mm, which is 60 % greater than that of OPC [11]. However, as the carbonation progresses, carbonation products will close the pores [12,13], hindering further CO_2 diffusion [14]. The carbonation of both OPC and SSC is typically limited to a surface depth of 5–10 mm [15,16], which greatly limits the CO_2 sequestration capacity, leading to a significant discrepancy between actual and theoretical carbon fixation.

The construction of an appropriate pore structure within the system

---

* Corresponding author at: School of Materials Science and Engineering, Southeast University, Nanjing, Jiangsu 211189, China.
** Corresponding author.
E-mail addresses: 2698977751@qq.com (S. Xiao), c.chang-1@tudelft.nl (C. Chang).

https://doi.org/10.1016/j.conbuildmat.2025.142475
Received 12 March 2025; Received in revised form 25 June 2025; Accepted 26 June 2025

can significantly improve the depth of CO_2 transport [17], but the distribution of pore sizes will notably impact the mechanical performance of the system [18,19]. Studies indicate that the micron-pore range beneficial for CO_2 transport is 1–100 μm [20,21], but pores within this range may cause substantial degradation of the system's mechanical properties [22,23]. Recent research has demonstrated that biochar can effectively increase carbonation depth without compromising mechanical properties by constructing micron-porous transport channels in the system[24]. Praneeth et al. [25] prepared bamboo-based biochar by pyrolyzing bamboo in an anaerobic environment at high temperatures, preserving the bamboo's interconnected porous microstructure. The channels in the biochar are not blocked by carbonation products. Biochar possesses inherent mechanical properties, and its incorporation at levels below 30 % does not adversely affect the performance of the system [26,27]. Additionally, biochar's large specific surface area can induce the nucleation of hydration products and promote hydration [28,29]. Furthermore, Gupta et al. [30] incorporated biochar pre-adsorbed with CO_2 into the paste to reduce carbon emissions by utilizing its CO_2 adsorption properties. Although biochar enhances carbonation depth, the improvement in carbon sequestration capacity is limited, because carbonation is difficult to extend laterally within the same depth.

Incorporating zeolite to construct a hierarchical pore structure can effectively overcome this limitation. Zeolite, an aluminosilicate mineral with a regular porous structure and molecular sieve characteristics [31], has been used by Ramezanianpour et al. [32] to enhance the carbonation depth of OPC by 230 % due to its nanometer-scale structure. The network formed by silica tetrahedra and alumina tetrahedra in zeolite allows CO_2 molecules to pass through and enables CO_2 adsorption [33,34], The physical adsorption capacity of CO_2 in zeolites with different crystal structures and aluminosilicate ratios ranges from 1.7 to 5 mmol/g [35]. The numerous pores around 10 nm in zeolite do not affect the system's strength but, rather, promote cement hydration through their large specific surface area [36], and construct CO_2 transport pathways within the dense matrix [37].

This study combines bamboo-based biochar (Bam) and zeolite (Zeo) to create an ideal pore structure that activates the carbonation potential of SSC and enhances its mechanical properties. In previous studies, most research mainly focused on the individual effects of the two and did not analyze the possible multi-level pore structure formed between them. Currently, the way to construct a multi-level pore structure in cement is mainly through the addition of admixtures or by using freezing. The multi-level pore structure mentioned in this paper does not require a complex forming process, greatly reducing production costs. The micropores of biochar facilitate the deep transport of CO_2, increasing the maximum carbonation depth, while zeolite creates pores in the dense matrix, allowing carbonation to extend laterally within the same depth, thereby maximizing CO_2 fixation. The research aims to evaluate the synergistic effects of both additives and provide new insights into the design and fabrication of ultra-low-carbon cementitious materials with high performance.

2. Material and methods

2.1. Materials

In this experiment, GGBS was used as the primary strength source, with semi-hydrated desulfurized gypsum as the sulfate activator. PI·42.5 cement, as the standard cement, can provide stable chemical properties and a uniform hydration process when verifying the performance of the system. Therefore, PI·42.5 Portland cement is selected as the alkaline activator to form a strength structure. The cement used in the experiment was supplied by Fushun Group, the semi-hydrated desulfurized gypsum was provided by Henan HENGSHENG Environment Co., Ltd., and the zeolite was supplied by Gongyi Hengxin Factory. The biochar used in this experiment was bamboo-based biochar, which was prepared by high-temperature pyrolysis of bamboo in an oxygen-free environment at 850℃, with nitrogen (N_2) used as a protective gas to prevent oxidation. Detailed information on raw materials is shown in the supply information.

The fine aggregate used in the mortar preparation was produced by Xiamen ISO Standard Sand Co., Ltd., with a particle size range of 0.5–1.0 mm, conforming to the Chinese ISO standard for sand. Additionally, the superplasticizer used in the experiment was produced by Sobute New Materials Co., Ltd. Polycarboxylic acid-based superplasticizer can significantly improve the mixing performance of cement without causing significant strength loss.

2.2. Sample preparation and methods

To evaluate the performance of composite materials, explore the optimal ratio of biochar and zeolite for their synergistic effect, and compare the effects of each component when acting alone, while keeping the carbon emissions as low as possible, the dosages of cement and gypsum were fixed at 2 wt% and 20 wt%, respectively. The dosage of biochar was fixed at 5 % to ensure workability, and the dosages of zeolite at 3 wt% and 5 wt% were attempted to see if they could form a good synergistic effect with it. Under the constant water-binder ratio (W/B) of 0.5, the mortar and paste were prepared according to the ratios shown in Tables 1 and 2, and the specimen dimensions are as shown in Fig. 1. After molding, all samples were placed in an environment with a temperature of 23 ± 2℃ and a relative humidity (RH) of ≥ 95 % for 24 h, followed by demolding and curing in the same environment until the required testing age was reached. The prepared samples were then crushed and immersed in isopropanol for 3 days to terminate the hydration process. Subsequently, the samples were vacuum-dried at 45℃ for 2 days and stored in vacuum-sealed bags for subsequent experiments.

The mechanical properties were tested in accordance with the requirements of GB/T 17671–2021, three mortar specimens were prepared for each group at curing ages of 3, 7, and 28 days. The specimens were molded and cured in standard conditions. The loading rates for the bending and compressive strength tests were maintained at 50 N/s and 2.4 kN/s, respectively.

Two carbonation regimes were used to characterize performance under different conditions, the relevant parameters of the two carbonization systems are shown in Fig. 1. The mortar specimens were cut at the midsection and sprayed with a 1.5 % phenolphthalein solution. The carbonation depth was measured at three points on each side, and the average depth of the uncolored area was recorded. Paste blocks are divided according to the depth from the surface as shown in Fig. 1. Samples were ground (<170 μm), and 2 g of powder was mixed with 20 g of water, stirred for 10 mins, and the solution's pH was measured after calibration with a pH= 7 buffer.

Phase quantification was performed using the internal standard based on Rietveld analysis. After single-sided carbonation, cement paste samples were taken every 5 mm. The samples were ground and sieved through a 200-mesh screen (r < 74μm). A mixture of 0.1 g α-Al_2O_3 and 0.9 g of powder was prepared using isopropanol, followed by vacuum drying at 40℃ for 24 h to obtain the sample for QXRD analysis.

The prepared samples were scanned using a Bruker D8 X-ray powder diffractometer. Nickel-filtered Cu-Kα radiation (λ=1.5405 Å, 40 kV, and 30 mA) was used at 23℃. X-ray diffraction scans were performed within the 5° to 80° 2θ range, with a step time of 0.3 s and a step size of 0.02°. XRD data were collected using the Bruker D8 Advanced Diffractometer and Lynxeye detector, and the resulting data were analyzed using the Bruker Diffrac plus EVA software. Phase identification was performed based on the Powder Diffraction File (PDF) database from the International Centre for Diffraction Data (ICDD). The obtained data were imported into TOPAS software for analysis, fitting, and normalization to determine the phase content. The remaining experimental procedures will be further described in the supply information.

Table 1
Mix proportions of paste.

Mix	Cement		Gypsum		Slag		Biochar		Zeolite		Water	
	wt%	g	wt%	g	wt%	g	wt%	g	wt%	g	W/B	g
OPC	100	500	0	0	0	0	0	0	0	0	0.5	250
Base	2	10	20	100	78	390	0	0	0	0	0.5	250
B5	2	10	20	100	73	365	5	25	0	0	0.5	250
Z5	2	10	20	100	73	365	0	0	5	25	0.5	250
Z3B5	2	10	20	100	70	350	5	25	3	15	0.5	250
Z5B5	2	10	20	100	68	340	5	25	5	25	0.5	250

Table 2
Mix proportions of mortar.

Mix	Cement/%		Gypsum/%		Slag/%		Biochar/%		Zeolite/%		Fine aggregate		SP/%		Water	
	wt%	g	wt%	g	wt%	g	wt%	g	wt%	g	Sand/Binder	g	wt%	g	W/B	g
Base	2	9	20	90	78	351	0	0	0	0	3:1	1350	0.2	0.9	0.5	225
B5	2	9	20	90	73	328.5	5	22.5	0	0	3:1	1350	0.2	0.9	0.5	225
Z5	2	9	20	90	73	328.5	0	0	5	22.5	3:1	1350	0.2	0.9	0.5	225
Z3B5	2	9	20	90	70	315	5	22.5	3	13.5	3:1	1350	0.2	0.9	0.5	225
Z5B5	2	9	20	90	68	306	5	22.5	5	22.5	3:1	1350	0.2	0.9	0.5	225

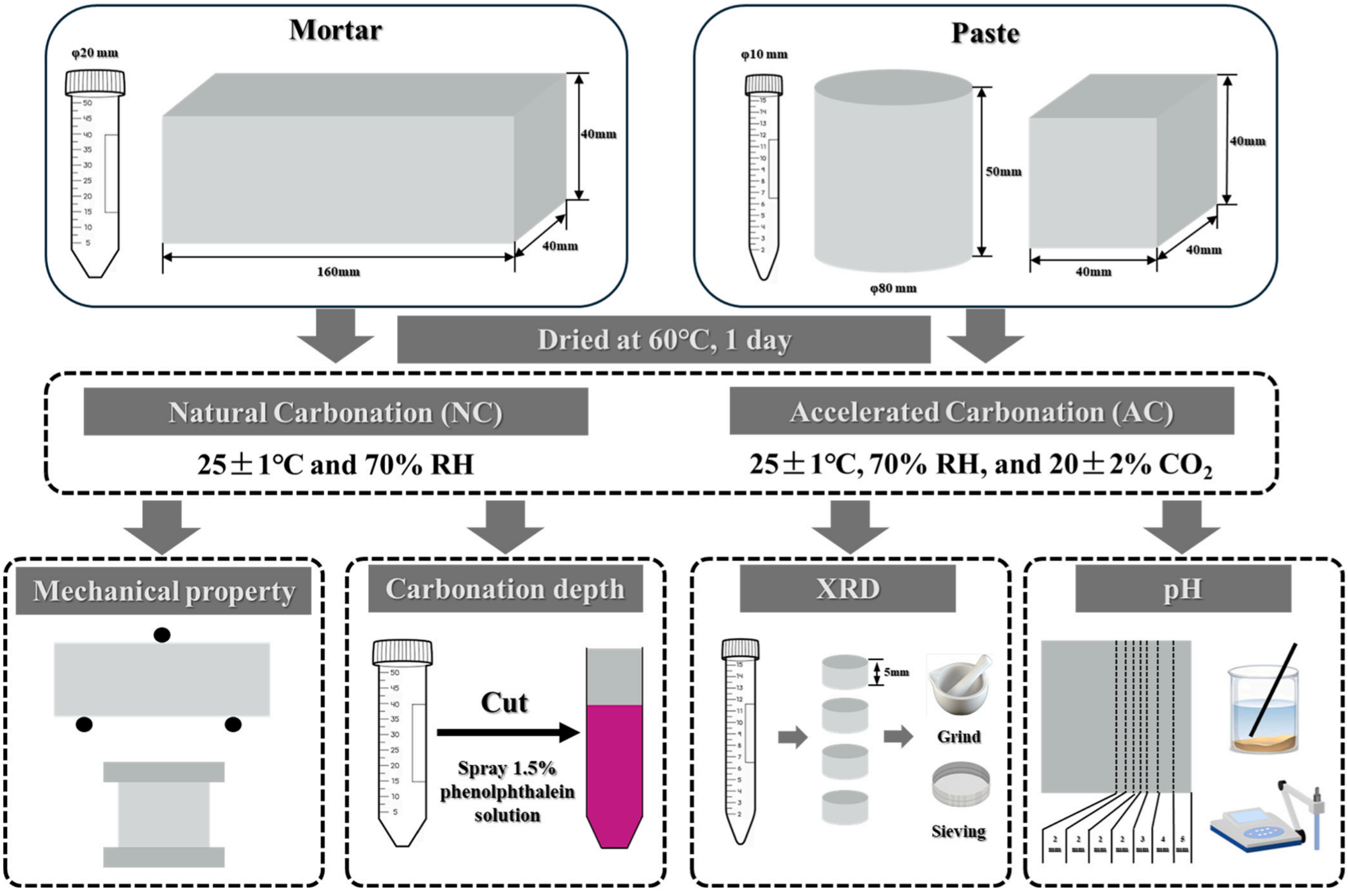

Fig. 1. Experimental process diagram.

2.3. *Finite element method (FEM) simulation*

The CO_2 seepage field in models with different porosities and base permeability coefficients was simulated using COMSOL, the detailed modeling process is described in the supply information. A transient simulation of a two-dimensional model was conducted using the Diluted Species Transport module. Two models with porosities of 25.76 % and 28.68 % were created based on the measured porosity from the experiments. The permeability coefficients of the pore and matrix (D_{pore}, D_{base}) were obtained from the literature [38,39]. The simulation was run over a time domain of 672 h (28 days) with a time step of 1 h, and all computations were performed on a laptop.

3. Results

3.1. Macroscopic performance

3.1.1. Mechanical property

The effect of Bam and Zeo on the strength of SSC mortar is shown in Fig. 2. Previous studies have demonstrated the positive impact of Bam incorporation on strength development, and in this experiment, the introduction of Bam also led to improvements in both compressive and flexural strength. The sole incorporation of Zeo also showed strengthening effects; however, due to its lack of hydration activity, the strength improvement is more likely attributed to its fineness, which contributes to densification and the catalytic effect on hydration due to its large surface area.

When both Bam and Zeo were incorporated into the SSC, significant improvements in the mechanical properties of the mortar were observed. After replacing 10 % of the slag, the Z5B5 group achieved compressive and flexural strengths of 31.15 MPa and 9.2 MPa at 28 days, which represented increases of 63.1 % and 43.8 %, respectively, compared to the Base group. Moreover, the mechanical properties of the composite were superior to the Base group at all ages, with significant differences starting to appear at 7 days as hydration progressed. The combined effect of Bam and Zeo was notably superior to their individual incorporation, and the strength of the composite system continued to increase with the increasing addition of Zeo, demonstrating a good synergistic effect.

3.1.2. Carbonation depth

The carbonation depth indicates the matrix's ability to absorb CO_2. The carbonation depths of SSC mortar under different carbonation curing regimes are shown in Fig. 3. Under NC conditions, all mortar samples, except Z5B5, had carbonation depths of less than 2 mm. The Z5B5 group reached 2.625 mm in 3 days and remained at 1.56 mm at 28 days, 40–150 % higher than the lowest carbonation depth in the SSC group. When Bam and Zeo were added separately, Bam significantly enhanced the CO_2 transmission rate, while Zeo also improved it, but to a lesser extent due to Zeo's densification effect on the matrix. Although Zeo allows CO_2 to permeate, it reduces micron-scale transport channels.

Fig. 3(b) shows carbonation depths under AC conditions, following the same trend as Fig. 3(a). The Z5B5 group's carbonation depth increased by 19.1–35.3 % compared to the Base group at 3–28 days and showed an 8.2–17.3 % improvement compared to the individual groups. The combination of Bam and Zeo resolved the densification issue caused by Zeo, micron-channel effectively enhancing CO_2 transport. The molecular sieve structure of Zeo also helped with CO_2 diffusion in the dense matrix, demonstrating their synergistic effect.

3.1.3. Gas permeability

Gas permeability testing is a key method for characterizing gas transport in materials [40]. The gas permeability coefficients and related parameters are summarized in Table 3. The Z5B5 group showed 75–100 % higher gas permeability than the Base group, indicating better transmission performance. At 7 and 28 days, carbonation reduced the permeability of the Base group by 20.5 % and 38.2 %, respectively, due to calcium carbonate ($CaCO_3$) microcrystals blocking micropores. In contrast, carbonation reduced the Z5B5 group's permeability by only 6.9 % and 14.8 %, maintaining CO_2 transmission channels and enabling deeper carbonation. The density increase after carbonation reflects CO_2 stabilization within the material. Across all conditions, Z5B5 consistently exhibited better gas permeability than the Base group.

3.2. Hydration process

The heat release curves of the five samples during hydration are shown in Figure 4 Fig. 4(a) illustrates the effects of Bam and Zeo on hydration rate. The first peak after the induction period represents the stage of the fastest formation of early hydration products [41]. Adding Bam advanced the main peak from 21 to 17 h and slightly increased its height, creating a 3-hour plateau around the peak, reflecting Bam's nucleation effect due to its high specific surface area. In contrast, Zeo delayed the main peak and reduced its height, as it lacks hydration activity and reduces overall hydration heat by replacing GGBS. The Z3B5 and Z5B5 groups benefited from Bam's earlier peak but showed reduced peak intensity due to the use of zeolite to replace the slag in the component.(Fig. 5)

The cumulative heat release, indicating hydration extent and strength potential [42,43], is shown in Fig. 4(b). In the first 40 h, Bam's nucleation effect increased cumulative heat release in the B5 and Z5B5 groups. By 3 days, Zeo's densification effect improved Z5B5's strength. At 120 h, Z5B5 reached 135 J/g, a 6.3 % increase over the Base group's 127 J/g, aligning with its superior 7-day strength.

Samples without carbonation treatment were soaked in isopropanol to remove free water, the mass difference before and after soaking was used to calculate the remaining w/b [44]. The remaining w/b is used to correct the QXRD results to ensure that the percentage results are correctly converted into the actual mass values.

3.3. Carbonation and CO_2 permeation mechanism

3.3.1. Pore structure

The carbonation-enhancement effect of OPC partly arises from the formation of $CaCO_3$ microcrystals during carbonation, which block micropores and hinder further CO_2 penetration. Simultaneously, the

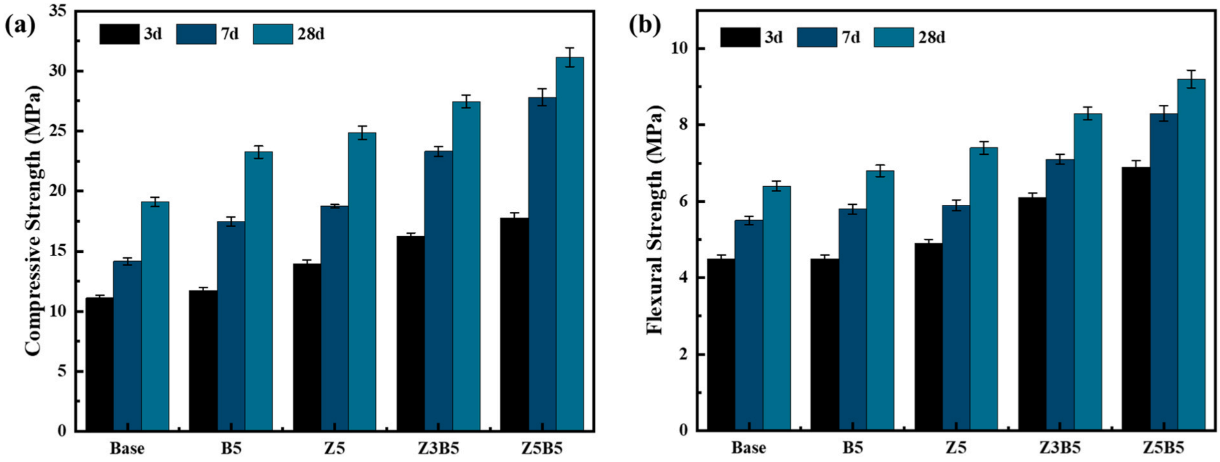

Fig. 2. Influence of Zeo and Bam on (a) compressive and (b) flexural strength of mortar.

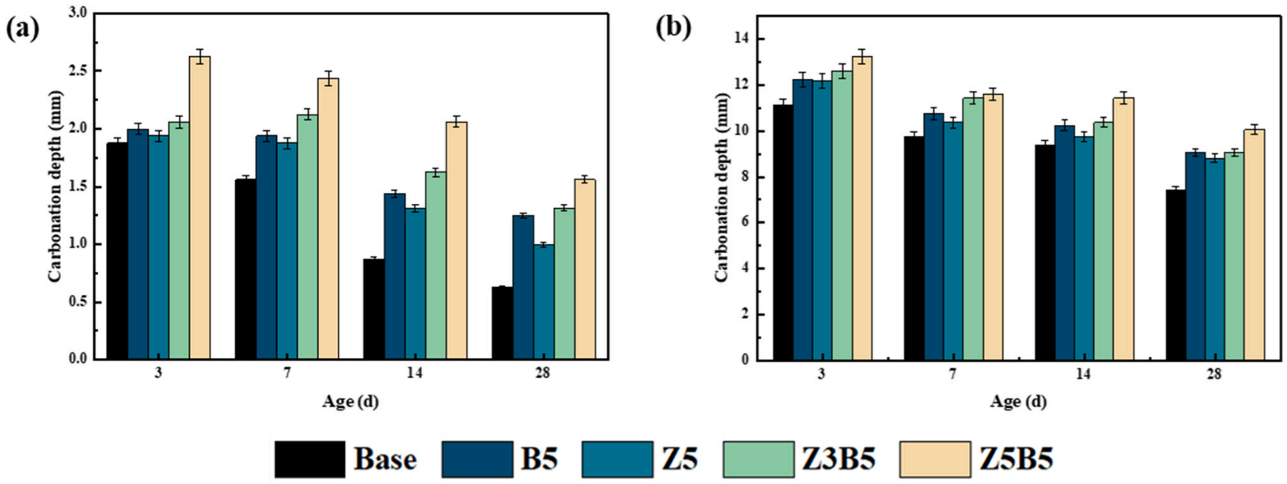

Fig. 3. Carbonation depth under (a) Natural carbonation (b) Accelerated carbonation.

Table 3
Nitrogen permeation measured gas permeability, porosity, and core skeleton density.

Name	Base-NC-7d	Base-AC-7d	Z5B5-NC-7d	Z5B5-AC-7d	Base-NC-28d	Base-AC-28d	Z5B5-NC-28d	Z5B5-AC-28d
Gas permeability (MD)	6.67	5.30	11.67	10.86	6.20	3.83	10.90	9.29
Porosity (%)	33.29	30.81	36.66	35.90	31.17	28.85	35.48	34.59
Core skeletal density (g/cm^3)	1.96	2.07	1.73	2.02	1.97	2.08		

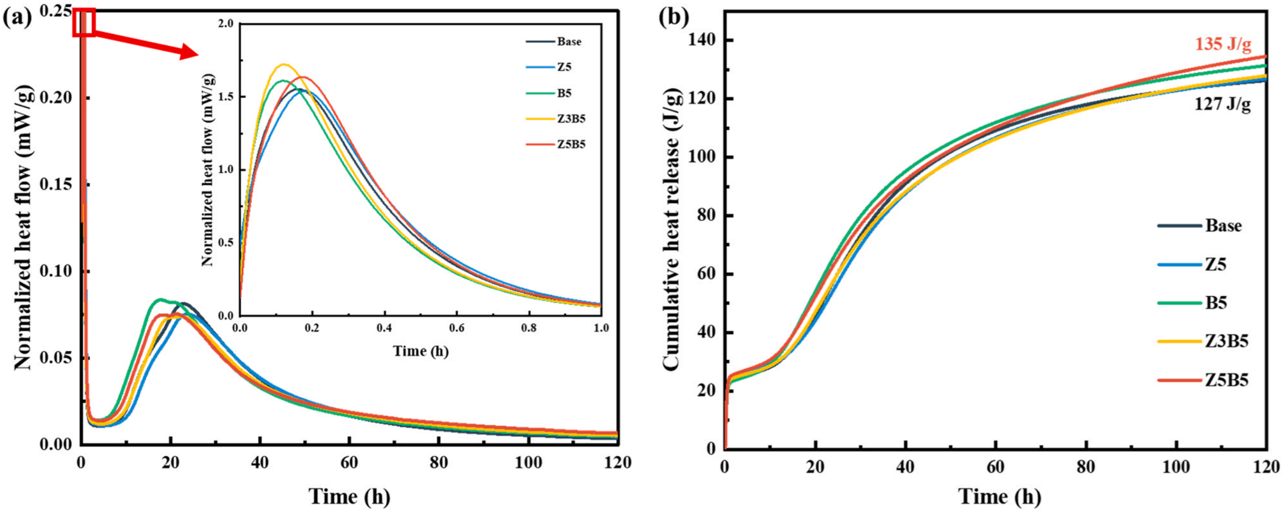

Fig. 4. Measured hydration heat: (a) heat flow and (b) the cumulative heat release.

distribution of porosity significantly influences the strength of the matrix [45]. To investigate the impacts of carbonation and the incorporation of Bam and Zeo on the pore structure, MIP tests were conducted. The results are shown in Fig. 6.

Fig. 6(a) and (b) illustrate the pore size distribution curves of different sample groups. Under uncarbonated conditions, the pore size distributions of Bam and Zeo when acting independently reveal their distinct influences on the pore structure. In the B5 group, the most probable pore diameter is centered around 200 nm, which is significantly smaller than the 700 nm observed in the Base group. However, the peak intensity does not show a notable reduction, and a more pronounced peak appears in the macropore region. This suggests that Bam enhances capillary pore densification through its hydration-promoting effect while simultaneously contributing to macroporosity due to its intrinsic structure. This behavior is consistent with previous findings, where Bam exhibited similar characteristics in OPC systems [46]. In contrast, the Z5 group shows a more pronounced pore refinement effect, with a significant reduction in peak intensity and the emergence of a higher number of gel pores around 10 nm. This indicates that Zeo, through its pozzolanic reaction, generates additional C-S-H, effectively densifying the pore structure. This observation aligns with the superior mechanical performance of the Z5 group. According to Powers' theory [47], gel pores do not adversely affect matrix strength. On the contrary, Zeo reduces the volume of strength-compromising pores and converts them into CO_2 transport channels that do not impair mechanical properties.

Fig. 6(c) and (d), showing cumulative pore volume distributions, and Fig. 6(e) and (f), depicting pore content variations, further substantiate the effects of Bam and Zeo, as well as the impact of carbonation. Zeo's incorporation significantly reduced pores in the 100–1000 nm range

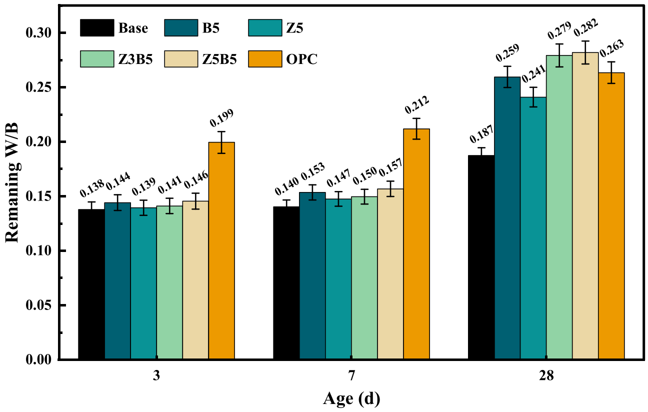

Fig. 5. Remaining W/B of paste at different ages.

while increasing the content of capillary pores. Bam contributed additional micron-pores, but its inherent strength mitigated the negative impact on the overall mechanical performance. Moreover, the individual incorporation of each material shows lower capillary pore content and total porosity. This can be ascribed to the adverse effect on workability induced by the combined water absorption characteristics of the two materials when used together, which leads to an increase in overall porosity in the blended system. In capillary pores larger than 100 nm, CO_2 reacts with hydration products on the pore wall surface, leading to the nucleation and growth of $CaCO_3$ microcrystals. This process gradually reduces the pore volume while increasing the proportion of pores within the 50–100 nm range through pore structure reorganization. Simultaneously, the carbonation-induced degradation of C-S-H phases increased the contents of capillary and gel pores. These findings suggest that the carbonation mechanism in this system differs from that of OPC and warrants further investigation in future studies.

3.3.2. QXRD and CO_2 carbonation coefficient

The dynamic process of carbonation was analyzed by performing QXRD tests at varying depths on specimens subjected to unidirectional carbonation under AC. The results, shown in Fig. 7, reveal distinct carbonation mechanisms between SSC and OPC systems. Due to its unique hydration mechanism, the SSC system lacks calcium hydroxide (CH), as corroborated by XRD results. In contrast, OPC, owing to its hydration characteristics, contains 18–20 wt% CH. As depicted in Fig. 7 (a) and (d), CH content in OPC significantly decreases within the 0–10 mm surface layer, indicating that CH serves as the primary source.

The SSC system, predominantly composed of AFt and CSH, contains approximately 20 wt% AFt in its matrix [48]. Fig. 7(b) and (e) show the depth-dependent changes in AFt content. At 3 days, the surface CH in OPC samples is entirely consumed, and carbonation continues to deplete some AFt. However, this phenomenon ceases by the 28-day mark. For SSC, AFt primarily drives the carbonation process. Near the surface, AFt is fully carbonated and progressively consumed as carbonation penetrates deeper into the core. The incorporation of Bam and Zeo further enhances AFt carbonation at comparable depths. As shown in Fig. 7(e), AFt content at a depth of 10 mm is reduced to nearly zero in SSC samples containing these additives. The sequence of carbonation reactions differs between the systems: CH > AFt > CSH for OPC and AFt > CSH for SSC. The degradation of the structural integrity in SSC after carbonation leads to a significant reduction in strength, whereas the structural framework in OPC remains largely intact. The conversion of CH to $CaCO_3$ in OPC contributes to a strength enhancement post-carbonation.

Regarding carbonation extent, OPC and SSC systems exhibit divergent trends, as illustrated in Fig. 7(c) and (f). The OPC system's denser matrix and abundance of CO_2-reactive mineral phases in the surface layers result in carbonation predominantly localized near the surface. Over time, this effect becomes more pronounced, with $CaCO_3$ formation confined within the top 5 mm and almost absent beyond 10 mm, as shown in Fig. 7(f). In contrast, SSC's relatively porous structure and sparse carbonation-reactive phases allow for a more uniform distribution of $CaCO_3$ throughout the 0–15 mm depth at both 3 and 28 days.

The combined addition of Bam and Zeo further enhances $CaCO_3$ formation at equivalent depths. With increasing Zeo content, the carbonation distribution curve remains consistent in shape but shifts upward, reflecting the synergistic effects of Bam and Zeo in promoting CO_2 transport. This observation aligns with earlier results, demonstrating the complementary role of these additives in enhancing carbonation.

From the $CaCO_3$ content data obtained via QXRD, the CO_2 uptake of 40 × 40 × 40 mm specimens can be calculated. Since the QXRD results represent mass percentages that include chemically bound water, and because the volume occupied at different depths varies, it is necessary to introduce relevant parameters for correction. The calculation process is outlined in Eq. (1), and the results are presented in Table 4.

In Eq. (1), R_r represents the remaining w/b, derived from the data in Fig. 5. M_b denotes the mass of the binder, uniformly set at 500 g. φ_{Vol}, depth is the volume fraction of each depth, calculated as 57.8 %, 29.7 %, 10.9 %, and 1.6 % for the four respective depths from the outer surface to the inner core. $M_{CaCO_3,\ wt\%}$ represents the mass percentage of $CaCO_3$ obtained from QXRD analysis.

Additionally, using the CaO content (excluding gypsum) measured by XRF, the theoretical maximum CO_2 uptake, assuming complete conversion of CaO to $CaCO_3$, can be calculated. By comparing the actual CO_2 uptake to this theoretical maximum, the degree of carbonation excluding deviations caused by changes in raw materials can be determined using Eqs. (2) and (3).

$$M_{absorption} = 0.44\sum R_r M_b \varphi_{Vol,depth} M_{CaCO_3,wt\%} \tag{1}$$

$$M_{ability} = \frac{11}{14}\sum M_{Content}\varphi_{CaO,wt\%} \tag{2}$$

$$R_{carbonation} = \frac{M_{absorption}}{M_{ability}} \times 100\% \tag{3}$$

In terms of CO_2 uptake, the Base group absorbed only 33.8 kg·CO_2/kg, significantly lower than the 68.7 kg·CO_2/kg observed for the OPC group. This discrepancy arises from the lower CaO content in the slag used within the SSC system. However, in terms of carbonation rate, both OPC and SSC exhibited a similar conversion rate of approximately 28 %, indicating no substantial difference in their actual CO_2 absorption capacity. This finding challenges the misconception that SSC is unsuitable as a basis for CCS technologies. In comparison, the incorporation of Bam and Zeo resulted in a steady increase in CO_2 uptake, even when they reduced the CaO content of the matrix. The Z5B5 group achieved a CO_2 uptake of 39 kg·CO_2/kg, representing a 15.4 % improvement over SSC. Notably, both Bam and Zeo significantly enhanced the carbonation rate. The Z5B5 group, which incorporated both, achieved a carbonation rate of 37 %, a 32.5 % improvement over SSC.

This calculation method eliminates interference from the raw materials, demonstrating that the observed increase in carbonation rate is solely attributable to changes in the CO_2 transport process within the matrix. Combined with the experimental results discussed earlier, this conclusively proves that the biochar-zeolite system we designed possesses excellent capabilities for both vertical penetration and lateral diffusion of CO_2. These enhancements significantly improve SSC's CO_2 uptake, enabling it to meet near-zero or even negative carbon emission targets.

4. Discussion

4.1. FEM transmission simulation

Previous studies have used FEM to simulate CO_2 transport within

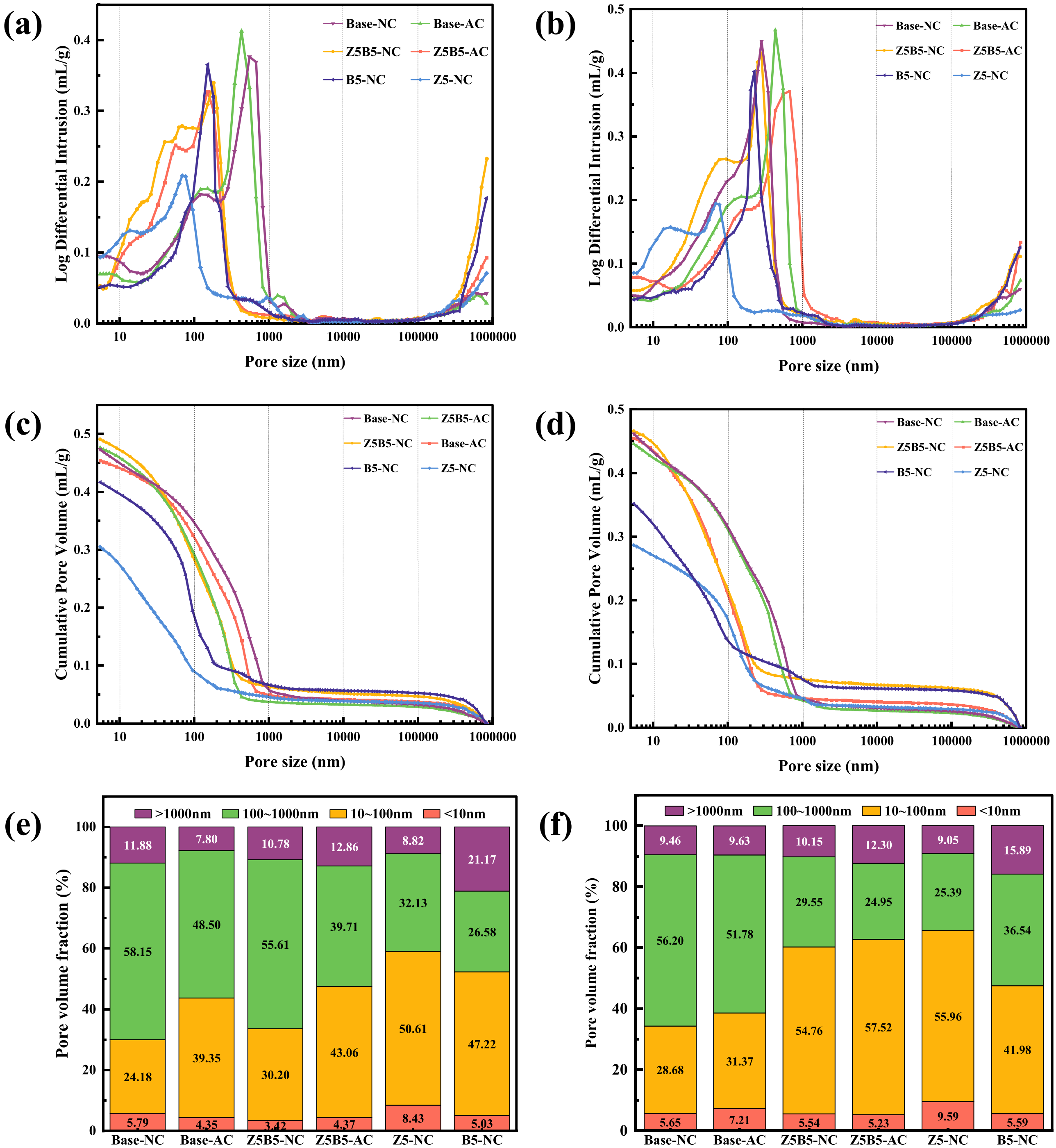

Fig. 6. Pore structure measured by MIP. Pore size distribution at (a) 7d (b) 28d ages; Cumulative pore volume at (c) 7d (d) 28d ages; Pore volume division at (e) 7d (f) 28d ages.

concrete [49]. Previous studies have shown that porosity plays a key role in CO_2 transport, with differences in porosity explaining variations in penetration depth. However, large-depth interconnected pores are unlikely. Gas transport between pores must pass through the dense matrix. This bottleneck effect makes matrix permeability the primary factor determining overall penetration depth. To validate this hypothesis, a COMSOL model was used to simulate CO_2 transport in porous media over 28 days. Four models were created by adjusting porosity and matrix permeability, corresponding to four experimental groups: 2576S (Base), 2576 F (Z5), 2868S (B5), and 2868 F (Z5B5). These group names will be referenced in the following discussion.

The visualization results in Fig. 8(b), reveal that models with higher porosity, such as B5 and Z5B5, exhibited slightly faster CO_2 diffusion compared to Base and Z5. However, the differences were minimal, as increased porosity only adds more connected pores rather than creating deep through-pores, which could compromise the cement matrix strength. In contrast, variations in matrix permeability had a significant impact, leading to notably greater penetration depths and faster movement of concentration contours. Thus, matrix permeability was clearly the more influential factor.

The average CO_2 concentration at different depths is shown in Figs. 8 (d) and 8(d). At 3 days, within the range of 200–400 mm, the Z5B5 group exhibited average CO_2 concentrations 44–50 % higher than the Base group. By 28 days, at a depth of 1000 mm, the CO_2 concentration in

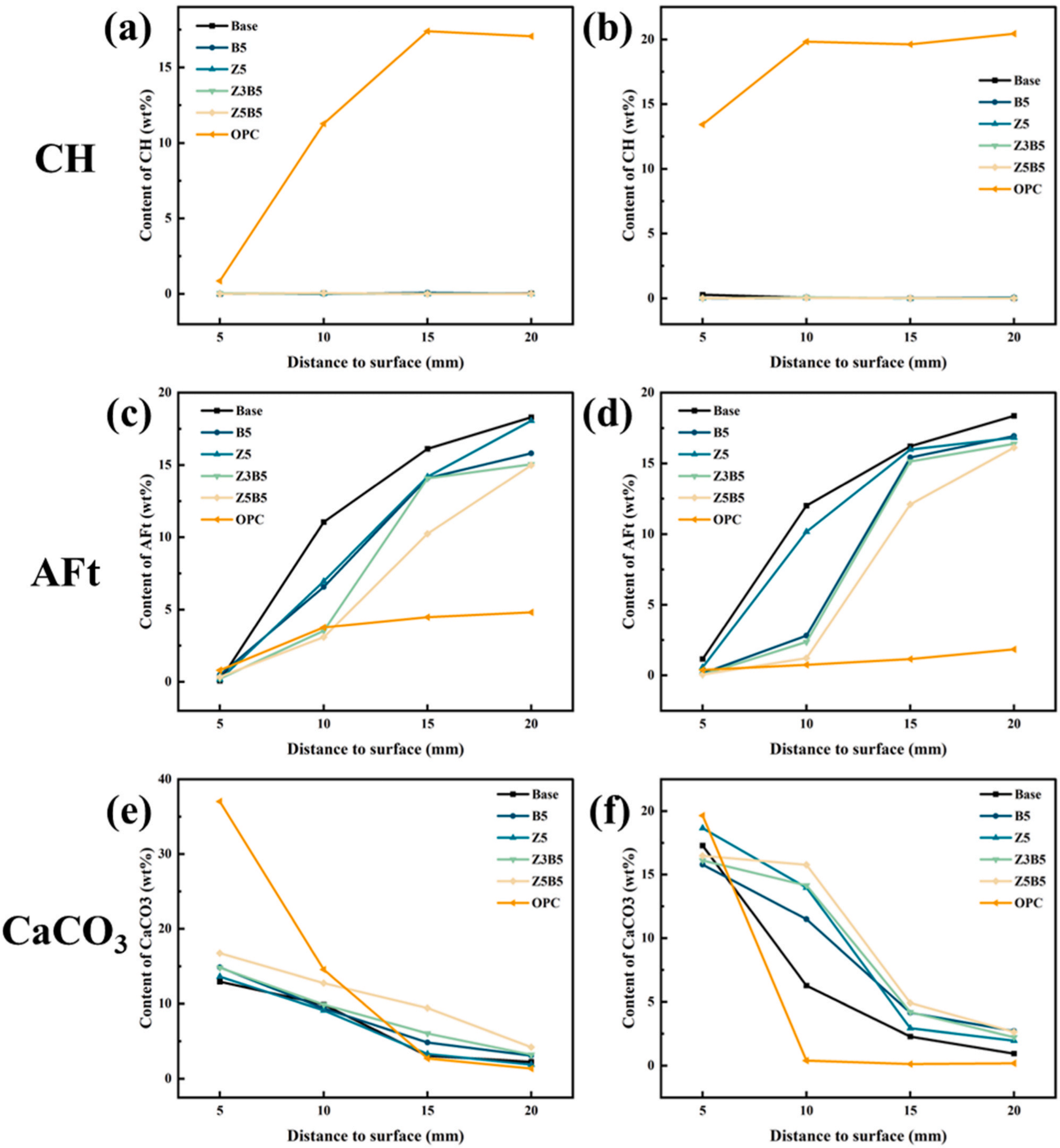

Fig. 7. Content of different phases in the paste at different ages measured by QXRD. $Ca(OH)_2$: (a) (b); AFt: (c) (d); $CaCO_3$: (e) (f).

Table 4
Theoretical maximum CO_2 absorption capacity, actual absorption capacity, and conversion rates of different systems.

Name	CO_2 absorption (kg·CO_2/kg)	Absorption ability (kg·CO_2/kg)	Carbonation rate (%)
OPC	68.72	245.97	27.94
SSC	33.82	122.26	27.66
B5	35.88	111.95	32.05
Z5	36.02	115.05	31.31
Z3B5	36.97	108.30	34.14
Z5B5	39.04	105.48	37.01

the Z5B5 group reached 4.6 mol/m^3 , a 206.7 % increase compared to the Base group (1.5 mol/m^3), and 119.1 % and 24.3 % higher than the B5 and Z5 groups, respectively. Meanwhile, B5 and Z5 achieved increases of 40 % and 146.7 %, respectively, compared to the Base group. The results demonstrate that the hierarchical pore structure effectively facilitates CO_2 transport, as shown in Fig. 8(a).

4.2. *Evaluation of CO_2 emission*

Given the complexity of accounting for transportation, processing, and other factors in a Life Cycle Assessment (LCA), significant variability in results is often observed. Here, the system’s carbon emissions per 500 kg of raw materials were evaluated using Global Warming Potential

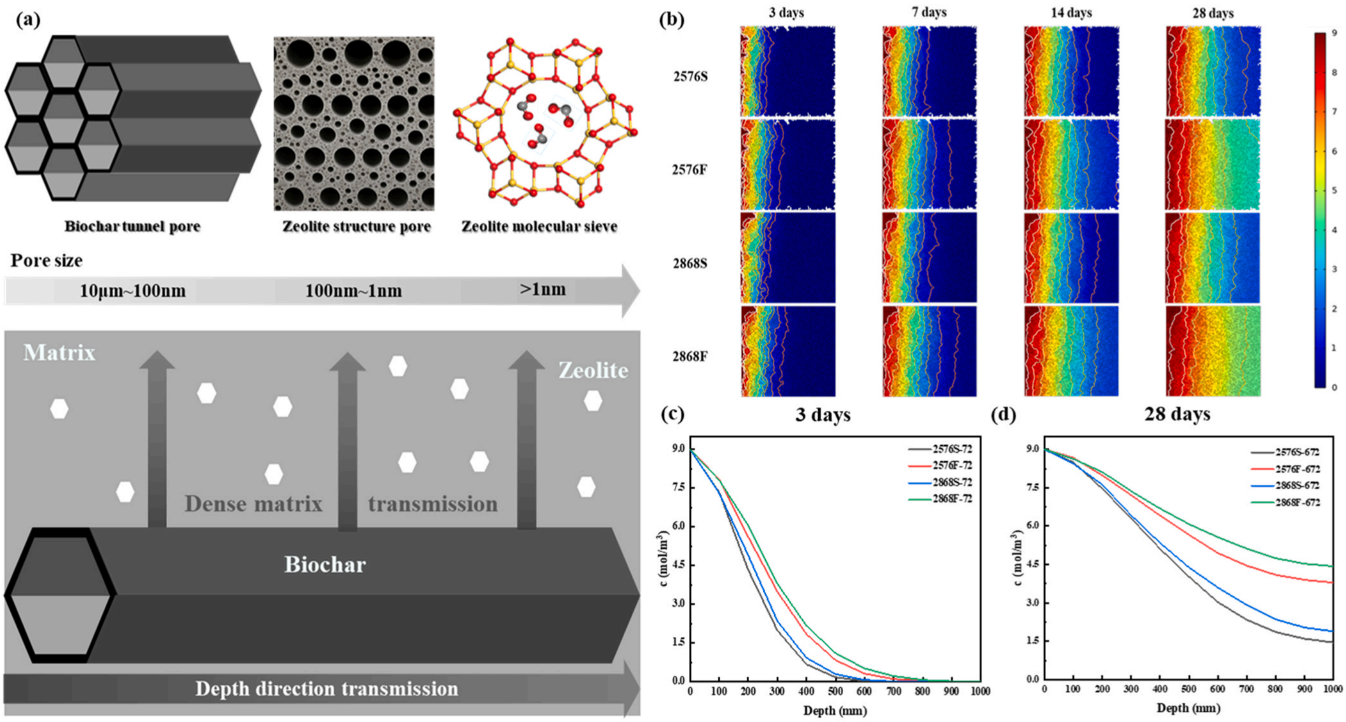

Fig. 8. Mechanism and FEM analysis results: (a) Mechanism schematic diagram; (b) Gas penetration depth and contour distribution; Gas concentration distribution at ages of (c) 7d, (d) 28d.

(GWP). The calculations were based on the material proportions employed in this study, with OPC composed entirely of cement, and SSC's composition referenced from the mixture design used by Chen et al. [50].

Campos et al. [51] estimated the life cycle carbon footprint of biochar to range from −1.4 to −0.7 kg·CO_2/kg, while Roberts et al. [52] reported a value of −0.864 kg·CO_2/kg. For this analysis, the value of −1.06 kg·CO_2/kg from Zhu et al. [53] was adopted. Zeolite, as a naturally occurring mineral requiring only grinding, was assigned a carbon emission factor of 0.06 kg·CO_2/kg, following the estimates provided by Chen et al. [54]. The results are summarized in Table 5.

Compared to mainstream low-carbon cementitious materials, LC3 cement reduces carbon emissions by about 30 % relative to OPC [55], while incorporating fly ash can achieve up to a 10 % reduction [56]. By introducing Zeo and Bam, carbon emissions can be reduced to 92.78 kg·CO_2/kg, representing reductions of 79.9 % and 32.8 % compared to SSC and OPC, respectively. This baseline carbon footprint surpasses most conventional cementitious systems.

The hierarchical pore structure also enhances CO_2 transport and absorption. OPC matrices and SSC systems typically limit carbonation to within 10 mm of the surface, restricting CO_2 sequestration. The mass transfer pathways established by Zeo and Bam allow CO_2 to penetrate deeper into the matrix without compromising structural integrity. Additionally, the hydration-promoting effects of Zeo and Bam accelerate the release of Ca phases, boosting carbon fixation potential. For instance, the Z5B5 mixture achieves a CO_2 sequestration capacity of 41.7 kg·CO_2/kg, a 24.6 % increase over conventional SSC (33.46 kg·CO_2/kg). This demonstrates the potential of hierarchical pore structure SSC systems as a viable pathway toward negative-carbon construction materials.

4.3. Limitations and research prospects

Compared to other low-carbon cement technologies, the carbon fixation approach used in this study facilitates large-scale industrial production without the need for additional infrastructure. It integrates the utilization of both industrial and agricultural waste, leveraging the intrinsic microstructure of materials to replace complex processing methods, thereby reducing the additional carbon emissions that might be generated during such processes. Moreover, the materials used are cost-effective, readily available, and enable the large-scale application of natural resources, resulting in significant economic benefits.

While this study demonstrates the significant potential of biochar and zeolite to enhance the performance and carbon sequestration

Table 5
Proportion of CO_2 emissions from various components of binder materials through GWP.

	Emissions (kg·CO_2/kg)	OPC	SSC	SSC-B5	SSC-Z5	SSC-Z3B5	SSC-Z5B5
GGBS	0.28	-	105	102.2	102.2	98	95.2
Gypsum	0.088	-	8.8	8.8	8.8	8.8	8.8
Cement	0.92	460	23	9.2	9.2	9.2	9.2
Biochar	−0.864	-	-	−21.6	-	−21.6	−21.6
Zeolite	0.012	-	-	-	0.3	0.18	0.3
SP	1.1	2.2	2.2	2.2	2.2	2.2	2.2
Water	4.3 × 10–4	0.08	0.08	0.08	0.08	0.08	0.08
Total (kg·CO_2/kg)	-	461.18	137.98	99.78	121.38	95.58	92.78
CO_2 absorption (kg·CO_2/kg)	-	68.72	33.46	37.66	37.19	39.42	41.7
Net emissions (kg·CO_2/kg)	-	392.46	104.52	62.12	84.19	56.16	51.08

capacity of SSC, certain limitations need to be addressed:

Environmental and Economic Trade-offs: Although the system effectively reduces carbon emissions, the extensive application and large-scale consumption of slag result in significant economic costs and a higher carbon emission potential. Therefore, it is essential to explore alternative industrial waste materials to replace slag. In future research, steel slag, which is challenging to fully utilize due to its high free-CaO content, will be a key focus. Additionally, carbide slag will be studied as a substitute for cement to serve as an alkaline activator, aiming to develop a fully waste-based carbon-negative cementitious material system.

Long-Term Durability: Although the composite's short-term mechanical performance and carbonation behavior are promising, however, under real environmental conditions, the performance of this material will be influenced by multiple factors. Durability properties such as freeze-thaw resistance, shrinkage, and chloride ion penetration resistance will play a critical role in determining its service life. These long-term durability aspects have not been fully evaluated, which is crucial for optimizing its carbon emissions over the entire lifecycle.

By addressing these areas, future studies can build upon the current findings to advance the practical application of near-zero-carbon SSC composites and further contribute to achieving negative-carbon cement production.

5. Conclusion

This study explores the incorporation of bamboo-based biochar and zeolite in the SSC system and aims to create a hierarchical pore structure that enhances CO_2 transport without compromising mechanical performance. The main conclusions are as follows:

(1) The combined incorporation of biochar and zeolite significantly enhances the mechanical properties of SSC due to the hydration promotion, up to an increase of 63.1 % and 43.8 % in compressive and flexural strength, respectively. The sole addition of biochar increases the cumulative heat release of SSC by 6.3 % over 120 h. Additionally, zeolite compacts the pores, reducing the content of capillary pores and decreasing the 100–1000 nm pore content by 20 % at 28 days.

(2) Biochar and zeolite play distinct roles in facilitating the CO_2 transport, through micro-scale channels and nano-level pores, promoting both vertical and horizontal carbonation, respectively. The co-incorporation of biochar and zeolite (Z5B5 group) increases carbonation depth by 19.1 %-35.3 % from 3 to 28 days. Simultaneously, the gas transmission rate improves by 75 %-100 %, while the permeability coefficient reduction caused by carbonation is significantly mitigated. It is further demonstrated by the FEM results. Due to the hierarchical pore structure, the CO_2 concentration at 1000 mm after 28 days increased by 206.7 % compared to the Base group, and by 119.1 % and 24.3 % compared to the single-addition groups.

(3) The co-incorporation of biochar and zeolite increases CO_2 absorption by 15.4 % and raises the carbonation rate from 27 % to 37 %, due to the dissolution promotion of Ca phases and CO_2 transport enhancement. As a result, GWP evaluation shows that the carbon emissions amount to 51.08 $kg \cdot CO_2/kg$, which is a reduction of 87 % and 51.1 % compared to OPC and SSC, respectively. In the future, based on this design strategy, negative-carbon emission may be achieved by utilizing higher CaO content solid waste in the raw materials.

CRediT authorship contribution statement

Wentao Chen: Writing – review & editing, Project administration, Formal analysis. **Jianxiong Miao:** Project administration, Methodology, Investigation, Formal analysis, Data curation, Conceptualization. **Shuai Xiao:** Writing – original draft, Visualization, Validation, Investigation. **ZHOU YANG:** Writing – review & editing, Project administration, Funding acquisition, Conceptualization. **Cheng Chang:** Project administration, Data curation. **Hao Zhang:** Project administration, Investigation. **Yanji Jin:** Project administration, Formal analysis, Data curation. **Luqing Cheng:** Project administration, Formal analysis, Data curation.

Funding

The authors acknowledge support from the National Key R&D Program of China (Grant No. 2023YFB3711400), the National Natural Science Foundation of China (Grant No. 52379120), the Natural Science Foundation of Jiangsu Province (Grant No. BK20230086) and the financial funding of Shandong High Speed Group Co., Ltd.

Declaration of Competing Interest

The authors declare that they have no known competing financial interests or personal relationships that could have appeared to influence the work reported in this paper.

Acknowledgement

The authors acknowledge support from the National Key R&D Program of China (Grant No. 2023YFB3711400), the National Natural Science Foundation of China (Grant No. 52379120), the Natural Science Foundation of Jiangsu Province (Grant No. BK20230086) and the financial funding of Shandong High Speed Group Co., Ltd.

Appendix A. Supporting information

Supplementary data associated with this article can be found in the online version at doi:10.1016/j.conbuildmat.2025.142475.

Data availability

Data will be made available on request.

References

[1] F. Winnefeld, et al., CO2 storage in cement and concrete by mineral carbonation, Curr. Opin. Green. Sustain. Chem. 38 (2022) 100672.
[2] A. Dixit, et al., Carbon capture in ultra-high performance concrete using pressurized CO2 curing, Constr. Build. Mater. 288 (2021) 123076.
[3] S. Griffiths, et al., Decarbonizing the cement and concrete industry: a systematic review of socio-technical systems, technological innovations, and policy options, Renew. Sustain. Energy Rev. 180 (2023) 113291.
[4] W. Lin, et al., A Biomimetic Cement-Based Solid-State Electrolyte with Both High Strength and Ionic Conductivity for Self-Energy-Storage Buildings, Research 7 0379.
[5] Y. Chen, et al., Multi-layered cement-hydrogel composite with high toughness, low thermal conductivity, and self-healing capability, Nat. Commun. 14 (1) (2023) 3438.
[6] T. Watari, et al., Efficient use of cement and concrete to reduce reliance on supply-side technologies for net-zero emissions, Nat. Commun. 13 (1) (2022) 4158.
[7] J.G. Driver, et al., Global decarbonization potential of CO2 mineralization in concrete materials, Proc. Natl. Acad. Sci. 121 (29) (2024) e2313475121.
[8] A. Gruskovnjak, et al., Hydration mechanisms of super sulphated slag cement, Cem. Concr. Res. 38 (7) (2008) 983–992.
[9] Y. Xie, et al., The impact of carbonation at different CO2 concentrations on the microstructure of phosphogypsum-based supersulfated cement paste, Constr. Build. Mater. 340 (2022) 127823.
[10] B. Yu, et al., Carbonation of supersulfated cement concrete after 8 years of natural exposure, Cem. Concr. Compos. 142 (2023) 105165.
[11] Y. Zhou, et al., The influence of two types of alkali activators on the microstructure and performance of supersulfated cement concrete： mitigating the strength and carbonation resistance, Cem. Concr. Compos. 118 (2021) 103947.
[12] M. Zajac, et al., Mechanisms of carbonation hydration hardening in Portland cements, Cem. Concr. Res. 152 (2022) 106687.
[13] M. Zajac, et al., Enforced carbonation of cementitious materials, Cem. Concr. Res. 174 (2023) 107285.
[14] P. Liu, et al., Carbonation depth model and carbonated acceleration rate of concrete under different environment, Cem. Concr. Compos. 114 (2020) 103736.

[15] D. Lu, et al., Innovative approaches, challenges, and future directions for utilizing carbon dioxide in sustainable concrete production, J. Build. Eng. 97 (2024) 110904.

[16] L. Li, M. Wu, An overview of utilizing CO2 for accelerated carbonation treatment in the concrete industry, J. CO2 Util. 60 (2022) 102000.

[17] B.K. Nyame, J.M. Illston, Relationships between permeability and pore structure of hardened cement paste, Mag. Concr. Res. 33 (116) (1981) 139–146.

[18] L. Bágel, V. Živica, Relationship between pore structure and permeability of hardened cement mortars: On the choice of effective pore structure parameter, Cem. Concr. Res. 27 (8) (1997) 1225–1235.

[19] S. Care, F. Derkx, Determination of relevant parameters influencing gas permeability of mortars, Constr. Build. Mater. 25 (3) (2011) 1248–1256.

[20] L. Leng, et al., An overview on engineering the surface area and porosity of biochar, Sci. Total Environ. 763 (2021) 144204.

[21] Q. Rusheng, et al., Various gas transport properties in concrete considering transporting mechanisms and testing methods-A review, Constr. Build. Mater. 389 (2023) 131636.

[22] J. Xiao, et al., Pore structure characteristics, modulation and its effect on concrete properties: A review, Constr. Build. Mater. 397 (2023) 132430.

[23] D. Xu, et al., The influence of curing regimes on hydration, microstructure and compressive strength of ultra-high performance concrete: A review, J. Build. Eng. 76 (2023) 107401.

[24] X. Chen, et al., Sludge biochar as a green additive in cement-based composites: Mechanical properties and hydration kinetics, Constr. Build. Mater. 262 (2020) 120723.

[25] S. Praneeth, et al., Accelerated carbonation of biochar reinforced cement-fly ash composites: enhancing and sequestering CO2 in building materials, Constr. Build. Mater. 244 (2020) 118363.

[26] L. Chen, et al., Biochar-augmented carbon-negative concrete, Chem. Eng. J. 431 (2022) 133946.

[27] X. Yang, X.-Y. Wang, Strength and durability improvements of biochar-blended mortar or paste using accelerated carbonation curing, J. CO2 Util. 54 (2021) 101766.

[28] S. Song, et al., Application of biochar cement-based materials for carbon sequestration, Constr. Build. Mater. 405 (2023) 133373.

[29] C. Zhao, et al., Activation of peroxymonosulfate by biochar-based catalysts and applications in the degradation of organic contaminants: a review, Chem. Eng. J. 416 (2021) 128829.

[30] S. Gupta, Carbon sequestration in cementitious matrix containing pyrogenic carbon from waste biomass: a comparison of external and internal carbonation approach, J. Build. Eng. 43 (2021) 102910.

[31] A. Ramesh Bura, B. Kondraivendhan, Effect of accelerated carbonation on the performance of concrete containing natural zeolite, J. Mater. Civ. Eng. 32 (4) (2020) 04020037.

[32] A.A. Ramezanianpour, et al., Micro and macro level properties of natural zeolite contained concretes, Constr. Build. Mater. 101 (2015) 347–358.

[33] M. Kong, et al., A review on development of post-combustion CO2 capture technologies: performance of carbon-based, zeolites and MOFs adsorbents, Fuel 371 (2024) 132103.

[34] P. Pasabeyoglu, et al., Solar-driven calcination of clays for sustainable zeolite production: CO2 capture performance at ambient conditions, J. Clean. Prod. 477 (2024) 143838.

[35] S. Kumar, et al., Utilization of zeolites as CO2 capturing agents: advances and future perspectives, J. CO2 Util. 41 (2020) 101251.

[36] Y. Tan, et al., Effects of superabsorbent polymer and natural zeolite on shrinkage, mechanical properties, and porosity in ultra-high performance concretes, Dev. Built Environ. 20 (2024) 100568.

[37] F. Sinngu, et al., Effects of natural zeolite on mechanical properties and durability indexes of concrete, Proc. Inst. Civ. Eng. Constr. Mater. 177 (5) (2024) 321–333.

[38] N. Seigneur, et al., Modelling of the evolving contributions of gas transport, cracks and chemical kinetics during atmospheric carbonation of hydrated C3S and C-S-H pastes, Cem. Concr. Res. 160 (2022) 106906.

[39] T. Häkkinen, The influence of slag content on the microstructure, permeability and mechanical properties of concrete: Part 2 technical properties and theoretical examinations, Cem. Concr. Res. 23 (3) (1993) 518–530.

[40] Q. Gui, et al., Gas permeability and electrical conductivity of structural concretes: Impact of pore structure and pore saturation, Cem. Concr. Res. 89 (2016) 109–119.

[41] H. Zhao, et al., Experimental and theoretical analysis on coupled effect of hydration, temperature and humidity in early-age cement-based materials, Int. J. Heat. Mass Transf. 146 (2020) 118784.

[42] S. Kourounis, et al., Properties and hydration of blended cements with steelmaking slag, Cem. Concr. Res. 37 (6) (2007) 815–822.

[43] N.C. Collier, et al., The suitability of a supersulfated cement for nuclear waste immobilisation, J. Nucl. Mater. 452 (1) (2014) 457–464.

[44] H. Feng, et al., Capillary water transport performance of cellulose nanocrystal modified cement/fly ash pastes with various water/binder ratios, Constr. Build. Mater. 450 (2024) 138694.

[45] G.M. Kim, et al., Reaction and microstructural characteristics of OPC pastes with low-lime calcium silicate cements under carbonation curing, Constr. Build. Mater. 415 (2024) 134993.

[46] J.J. Chen, et al., Solubility and structure of calcium silicate hydrate, Cem. Concr. Res. 34 (9) (2004) 1499–1519.

[47] A. Jafari, P. Sadeghian, Influence of biochar and recycled gypsum on the strength and microstructure of conventional and sustainable cementitious composites, Constr. Build. Mater. 408 (2023) 133715.

[48] J. Xing, et al., The influence of different kinds of weak acid salts on the macro-performance, micro-structure, and hydration mechanism of the supersulfated cement, J. Build. Eng. 66 (2023) 105937.

[49] S. Kashef-Haghighi, et al., Mathematical modeling of CO2 uptake by concrete during accelerated carbonation curing, Cem. Concr. Res. 67 (2015) 1–10.

[50] W. Chen, et al., Impact of basic oxygen furnace slag on the hydration microstructure, mechanical properties, and carbon emissions of supersulfated cement, Constr. Build. Mater. 432 (2024) 136673.

[51] J. Campos, et al., Life cycle assessment of biochar as a partial replacement to Portland cement. IOP Conference Series: Earth and Environmental Science, IOP Publishing, 2020 012025.

[52] K.G. Roberts, et al., Life Cycle Assessment of Biochar Systems: Estimating the Energetic, Economic, and Climate Change Potential, Environ. Sci. Technol. 44 (2) (2010) 827–833.

[53] X. Zhu, et al., Life-cycle assessment of pyrolysis processes for sustainable production of biochar from agro-residues, Bioresour. Technol. 360 (2022) 127601.

[54] X. Chen, et al., Comparative environmental assessment of zeolites synthesized from chemicals and natural minerals††Electronic supplementary information (ESI) available. See DOI: https://doi.org/10.1039/d3gc05146c, Green Chemistry 26(9) (2024) 5273-5283.

[55] P. Cong, et al., Comparison and assessment of carbon dioxide emissions between alkali-activated materials and OPC cement concrete, J. Traffic Transp. Eng. Engl. Ed. 11 (5) (2024) 918–938.

[56] R. Gettu, et al., Influence of supplementary cementitious materials on the sustainability parameters of cements and concretes in the Indian context, Mater. Struct. 52 (1) (2019) 10.